ADVANCED MATERIALS

www.advmat.de

Biomimetic Omnidirectional Antireflective Glass via Direct Ultrafast Laser Nanostructuring

*Antonis Papadopoulos, Evangelos Skoulas, Alexandros Mimidis, George Perrakis, George Kenanakis, George D. Tsibidis, and Emmanuel Stratakis**

Here, a single-step, biomimetic approach for the realization of omnidirectional transparent antireflective glass is reported. In particular, it is shown that circularly polarized ultrashort laser pulses produce self-organized nanopillar structures on fused silica (SiO_2). The laser-induced nanostructures are selectively textured on the glass surface in order to mimic the spatial randomness, pillar-like morphology, as well as the remarkable antireflection properties found on the wings of the glasswing butterfly, *Greta oto*, and various Cicada species. The artificial structures exhibit impressive antireflective properties, both in the visible and infrared frequency ranges, which are remarkably stable over time. Accordingly, the laser-processed glass surfaces show reflectivity smaller than 1% for various angles of incidence in the visible spectrum for s–p linearly polarized configurations. However, in the near-infrared spectrum, the laser-textured glass shows higher transmittance compared to the pristine. It is envisaged that the current results will revolutionize the technology of antireflective transparent surfaces and impact numerous applications from glass displays to optoelectronic devices.

There are numerous species in nature that exhibit extraordinary surface functionalities including plant leafs,[1,4] insects,[2–4] reptiles,[5] even elasmobranch fishes, and marine life.[4,6] These remarkable properties help those species to survive, feed, and thrive through extreme environmental conditions; their development has followed millions of years of evolution and the necessity of the species to evolve through natural selection. In most cases, the unconventional surface properties and attributes stem from their unique hierarchical morphological features, ranging from a few tens of nanometers to hundreds of micrometers in size.[7]

Based on the concepts and underlying principles discovered in nature, an interdisciplinary field has been developed, aiming to design and fabricate biomimetic structures.[7] Research in this field indicated several methodologies to develop bioinspired surfaces, exhibiting hierarchical structuring at the nano- and micro-lengthscales.[8–11] Laser fabrication is a maskless process allowing material modifications with a high precision over size and the shape of the fabricated features.[12] However, due to optical diffraction, the feature size resolution is limited to the order of wavelength (i.e., microscale); therefore, the challenge in biomimetic laser processing is to beat the diffraction limit and realize the structural complexity of natural surfaces, also, at the nanoscale. Materials' structuring using ultrashort (less than 1 ps) laser pulses, in particular, proved to be a precise and highly versatile tool to realize artificial surfaces that quantitatively mimic the morphological features and functionalities of their natural archetypes.[13–19] This capability comes as the outcome of the optimal combination of the ultrafast laser field and material properties that enable the production of features with sizes beyond the diffraction limit (i.e., nanoscale). A prominent example is the formation of self-organized subwavelength, laser-induced periodic surface structures (LIPSS), which have been proven an important asset for the fabrication of nanostructures with a plethora of geometrical features.[13,20–25]

This work is the first report on direct laser nanofabrication of biomimetic omnidirectional antireflective glass surfaces. It was inspired from the unique antireflection properties of the wings of the glasswing butterfly, *Greta oto*, and the Cicada *Cretensis* species.[2,3] This property is due to the presence of arrays (with periodicity in the range of 150–250 nm) of nonreflective nanosized (sub-100 nm size) pillars on both the top and the bottom surface of the wing. The current state-of-the-art technologies employed for the production of antireflection surfaces require either complex multiple steps and time-consuming procedures or chemical processes,[8,26–32] which, in some cases, produce hazardous wastes. At the same time, the chemical coatings' quality tends to degrade with time.[27,33,34] Here, we demonstrate a single-step laser texturing approach for the structuring of biomimetic antireflective nanopillars, on fused silica glass (SiO_2) surfaces. The overall properties of the produced surfaces were found remarkably similar to the natural butterfly and Cicada archetypes, both in terms of the surface morphology

A. Papadopoulos, E. Skoulas, A. Mimidis, G. Perrakis, Dr. G. Kenanakis, Dr. G. D. Tsibidis, Dr. E. Stratakis
Institute of Electronic Structure and Laser (IESL)
Foundation for Research and Technology (FORTH)
N. Plastira 100, Vassilika Vouton, 70013 Heraklion, Crete, Greece
E-mail: stratak@iesl.forth.gr

A. Papadopoulos, E. Skoulas, A. Mimidis, G. Perrakis, Dr. E. Stratakis
Materials Science and Technology Department
University of Crete
Vassilika Vouton, 71003 Heraklion, Crete, Greece

The ORCID identification number(s) for the author(s) of this article can be found under https://doi.org/10.1002/adma.201901123.

DOI: 10.1002/adma.201901123

and of functionality. The proposed technique is simple, low cost, chemicals free, and it can be easily scaled up using commercially available industrial laser-processing systems.[35,36]

Antireflective transparent materials can be useful for a wide range of technological applications including daily device screens,[37] solar windows,[38,39] optoelectronic devices,[40,41] and a plethora of optical components.[9,32,42,43] We envisage that the laser-based biomimetic fabrication approach presented here will have a huge impact on such applications, considering the simplicity of the process coupled with the durability of the antireflective structures attained.

Following irradiation of fused silica with a specific linearly polarized number of pulses (NP), the appropriate fluence (Fl) and high spatial frequency LIPSS (HSFL) are formed on the surface. The periodicity of HSFL is half, or less, of the laser wavelength λ, while their orientation is perpendicular to the incident polarization, as shown in **Figure 1**a. The physical mechanism that determines the size and orientation of HSFL in fused silica has been discussed in previews reports.[21,22,44] According to the most prominent explanation, the HSFL nanoripples' formation is due to the coherent superposition of the scattered near-field (evanescent) waves generated by single inhomogeneities, which are possibly irradiation remnants present on the material's surface.[44] The local field enhancement and eventual superposition of such scattered waves lead to periodic modulation perpendicular to the laser beam polarization.[44] An important feature of this mechanism is that nanoplasmas from randomly distributed inhomogeneities become oriented perpendicular to the laser polarization and evolve into self-organized HSFL patterns.

HSFL can be considered as a suitable structure for the production of antireflection surfaces in the visible, as their characteristic periodicity, obtained by 2D fast Fourier transform (2D-FFT) analysis, is 359 ± 24 nm, i.e., within the range of the periodicity exhibited by the array of nanopillars formed on the Cicada *Cretensis*[45] (**Figure 2**a) scales.

Notably, irradiation of fused silica with a specific number of circularly polarized pulses at 1026 nm, of appropriate fluence, gives rise to arrays of nanopillars (nanospikes), as shown by the respective scanning electron microscopy (SEM) images in Figure 1d. The respective 2D-FFT image confirms the uniform distribution of such nanospikes within the spot area. The size of nanospikes is controllable by the wavelength of the incident beam, although the periodicity remains unaffected (Figure S4, Supporting Information). The formation mechanism of nanopillars can be attributed to the characteristics of the circularly polarized laser light; more specifically, the equivalent contributions of the laser field components on the material's surface plane, due to circular polarization, cancel any periodic field modulation and subsequent pattern organization along a preferential direction.[46] As a result of the random distribution of nanoplasmas,[46] the laser-irradiated area is textured with an array of dots (see also Figure S8 in the Supporting Information), which are evolving into nanospikes upon irradiation with subsequent pulses.

A parametric study was conducted to identify the appropriate laser parameters required for the nanopillars formation. It is generally observed that, depending on the fluence used, nanospikes are formed for different number of pulses. For example at Fl = 6.1 J cm^{-2}, well-ordered nanospikes are formed for NP = 50, while at Fl = 6.6 J cm^{-2}, well-ordered nanopillars are

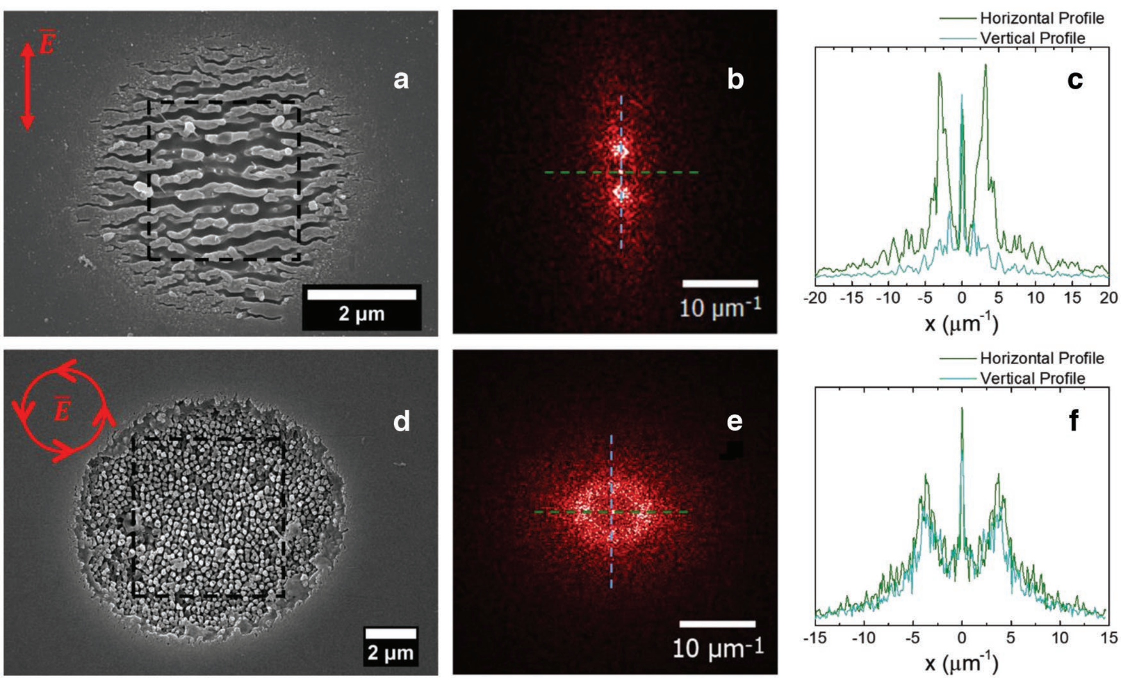

Figure 1. Polarization-dependent LIPSS. a,d) Top-view SEM image of fused silica surface. b,e) 2D Fourier transform (2D-FFT) of the area marked with the dashed black square. c,f) The profile of the dashed horizontal and vertical lines of b,e) Fourier transform, following irradiation with a–c) NP = 15 and λ = 1026 nm, linearly polarized pulses of Fl = 2.8 J cm^{-2}, and d–f) NP = 40 and λ = 1026 nm, circularly polarized pulses of Fl = 6.0 J cm^{-2}. The red arrows (in (a) and (d)) indicate the laser beam polarization.

ADVANCED MATERIALS
www.advmat.de

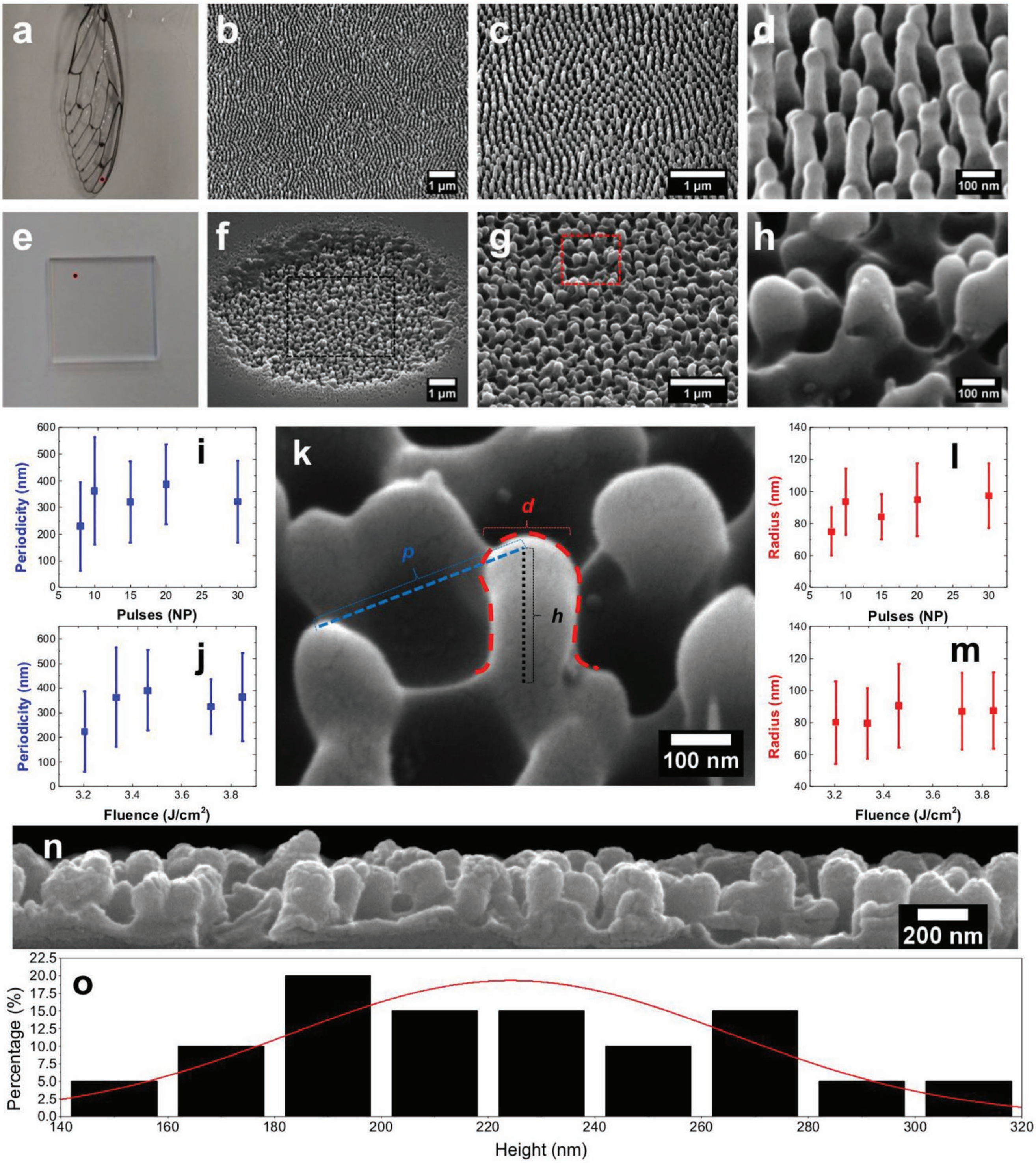

Figure 2. Natural versus biomimetic artificial surface and morphological characterization of the laser fabricated nanospikes. a–d) Photograph of a Cicada *Cretensis*[45] wing and respective SEM images (45° tilted) of the transparent antireflective area at different magnifications; the red spot indicates the SEM imaging area. e–h) Photograph of a fused silica plate and SEM images (45° tilted) of a spot fabricated on the surface using NP = 15 circularly polarized laser pulses of $\lambda = 1026$ nm wavelength, 1 kHz repetition rate with and170 fs pulse duration, of Fl = 6.8 J cm^{-2}; the red spot indicates the location of irradiation. i) Nanospikes' periodicity as a function of NP for Fl = 6.6 J cm^{-2}. j) Nanospikes' periodicity as a function of fluence for NP = 10. k) High-resolution SEM image (45° tilted) of a single nanospike. l) Nanospikes' radius as a function of NP for Fl = 6.6 J cm^{-2}. m) Nanospikes' radius as a function of fluence for NP = 10. n) Cross-sectional SEM image of the femtosecond laser-induced nanospikes. o) Height distribution.

formed for NP = 15, as shown in Figure 2b. By contrast, for NP > 50, no structures are produced, while a crater is formed instead. Hence, minor changes in fluence or in the number of pulses are strongly influencing the formation of nanospikes. The range of fluences where nanospikes are formed is Fl = 5.7–8.3 J cm^{-2}, while that of NP = 6–50 for the 1026 nm central wavelength. Moreover, the optimum pulse duration for the formation of nanospikes is below 5 ps. More information and the full map of structures obtained at various fluences and the number of pulses can be found in Figures S2 and S3 (Supporting Information).

To account for the periodicity, radius of curvature, and height of the fabricated nanospikes, a morphological analysis has been performed. The periodicity, in particular, calculated from 2D-FFT analysis of the corresponding SEM images and presented in Figure 2c,d, is estimated to be within the range of 200–400 nm. It can be observed that the pseudoperiodic character of those structures gives rise to a wide range of periodicities. However, as the fluence and number of pulses increase, the mean periodicity slightly increases. The nanospikes' radius, also calculated from the SEM images, shown in Figure 2f,g, was measured in the range of 70–100 nm. The radius values seem to be unaffected by the fluence changes; however, they increase slightly upon increasing the number of pulses. Finally, the average height of nanospikes was estimated, from cross-sectional SEM images, to be 224 ± 41 nm.

Toward the fabrication of large-area nanospike surfaces, a line scan study was initially attempted. It is observed that the homogeneous production of nanospikes, within the line, is quite challenging (see Figure S7 in the Supporting Information). In order to avoid the textures' inhomogeneities, the nanospikes were progressively formed using a series of consecutive scans (see Figure S8 in the Supporting Information). For the formation of the nanospikes in large areas, the sample was scanned in both directions and structuring is performed via the line-scan procedure described above. **Figure 3**a presents a picture of a fused silica plate processed in its central part to provide a square-shaped area of nanospikes (SEM images are provided in Figure S9 in the Supporting Information). The maximum area that can be textured using our setup was equal to 1 cm^2, as depicted in Figure 3a. It can be observed that under white light illumination, the laser-treated area is highly antireflective compared to the untreated outer peripheral area. The antireflection property of the processed areas has been confirmed by the respective reflectance spectra (Figure 3b,c) showing that it is more pronounced in the vis–NIR part of the spectrum. It is also found that the scanning lines' separation significantly affects the antireflection property (Figure S10, Supporting Information). In particular, as the percentage

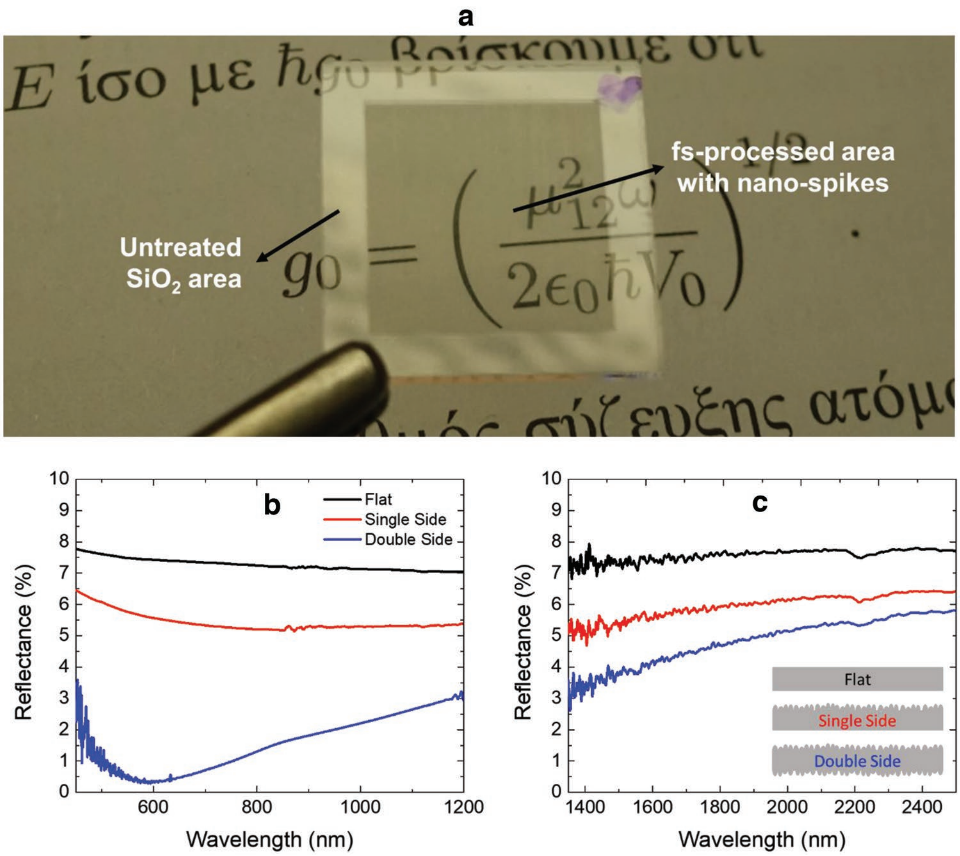

Figure 3. a) Photograph of a fused silica sample plate (the background is from the Greek translation of Quantum Optics by Mark Fox. and is reproduced with permission from Crete University Press), the central part of which was laser-treated to fabricate nanospikes; the black dashed rectangle indicates the processed area. b,c) Reflectance spectra of a pristine (black lines) and laser treated at one (red lines) or both sides (blue lines) of the fused silica plate. Laser processing has been performed using $N_{eff,2D}$ = 15 circularly polarized pulses (λ = 1026 nm, 1 kHz, 170 fs) with Fl = 5.8 J cm^{-2}.

coverage of nanospikes increases, the antireflection property is enhanced as well. Furthermore, as also shown in Figure 3b,c, the reflectivity was further decreased if both sides of the fused silica plate are laser-treated. Indicatively, the relative difference in reflectance between the untreated and the single-side processed plate is 1.7% for 1200 nm and 1.9% for 600 nm while that of the double-side processed one is 4.1% for 1200 nm and 7.1% for 600 nm, respectively. Such properties are comparable to those attained through the best antireflection technologies reported to date.[8,27]

Angle-resolved reflectance and transmittance spectra were recorded at three different wavelengths (445, 535, and 658 nm) for both s- and p-polarized light, using a custom-built angle-resolved reflectance spectroscope. The results are presented in **Figure 4**a and Figure 4b, respectively, for the untreated, single-, and double-side laser-processed fused silica

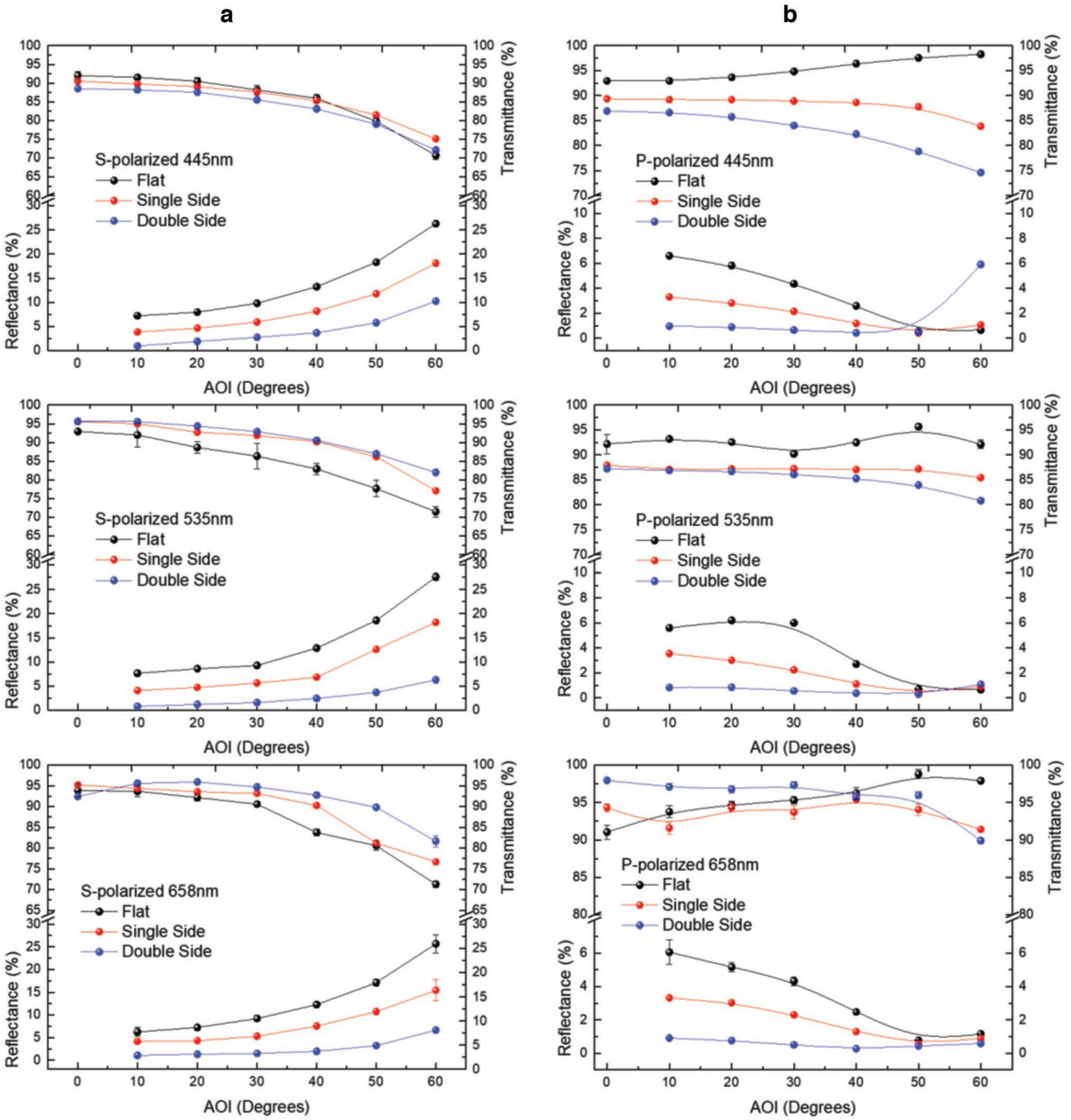

Figure 4. Transmittance and reflectance measurements for various AOI at 445, 535, and 658 nm wavelengths. a,b) Transmittance and reflectance measurements of "flat, single-side processed" and "double-side processed" fused silica for s-polarization (a) and p-polarization (b) configurations.

plate at various angles of incidence (AOI). It is observed that the reflectivity of single- and double-side processed fused silica plate is reduced compared to the bare one at practically all AOI and for all three wavelengths. Notably, the double-side processed material shows a significantly reduced reflectivity, which is less than 1%, for low AOI and less than 5% even at a large angle (i.e., 60°), which reveals remarkable omnidirectional antireflective property. Furthermore, the transmission is higher than 85% in all cases and slightly decreases for large angles. This result indicates the omnidirectional high transparency of the laser-processed fused silica plates. It should be emphasized that the observed omnidirectional antireflection properties are quite stable over time and remain at the same levels for at least 6 months after fabrication, upon storage in ambient conditions. This is a remarkable advantage of laser nanostructuring compared to the current state-of-the-art antireflection technologies.

To analyze the antireflection properties of laser-fabricated nanospikes, numerical simulations of light intensity distribution, as well as the angular dependence of reflection, were carried out. The simulations were conducted on a 1.3×0.65 μm^2 area, 1 mm thick, supercell comprising, on both sides, silica nanospikes of four different mean-valued dimensions, deduced from SEM images, as well as on a 0.328×0.328 μm^2, 1 mm thick, unit cell comprising, in both sides, a single type of silica nanospike for comparison; on the other hand, reflection calculations from a 1 mm silica slab with a flat surface were used for reference (see the Supporting Information and ref. [47]).

In **Figure 5**a–c, the calculated against the measured reflectivities were compared, as shown in Figure 4a,b, for the three different wavelengths and two polarizations. It is evident that regardless of the angle of incidence, the nanospikes' surface exhibits a decreased reflectivity by up to ten times compared to an untreated glass plate. Notably, the observed antireflective behavior can be attributed to the presence of nanospikes that induce a progressive transition of the effective refractive index, allowing effective coupling of light into the bulk of fused silica. This light-coupling effect is further indicated by the significantly enhanced intensity of light among the nanospikes (Figure 5d). Figures S11–S13 (Supporting Information) confirm that nanospikes can reduce the reflection by almost an order of magnitude, compared with the plane silica surface, for all wavelengths within the range of 400–800 nm. Moreover, comparing Figures S12 and S13 (Supporting Information) at spectral/angular regions where severe diffraction does not occur (i.e., 500–800 nm and 0°–30°), the four-nanospike supercell shows a more broadband reflection reduction compared to the unit cell with the single type of nanospike. This effect can be attributed to the nanospikes' randomness, which is found also to be behind the unique omnidirectional antireflection properties of the glasswing butterfly.[3]

In brief, we reported on a novel single-step and chemical-free technique for the fabrication of broadband, omnidirectional transparent antireflective surfaces, using ultrafast lasers. It is particularly demonstrated that irradiation of fused silica with circularly polarized femtosecond pulses gives rise to the formation of subwavelength-sized nanospikes on the materials' surface. Notably, and unlike most antireflection surfaces fabricated to date, the laser-induced nanospikes exhibit a quasiperiodic arrangement and present random height and width distributions, in a similar manner to the nanospikes found at the highly antireflective glasswing butterfly and Cicada wings.

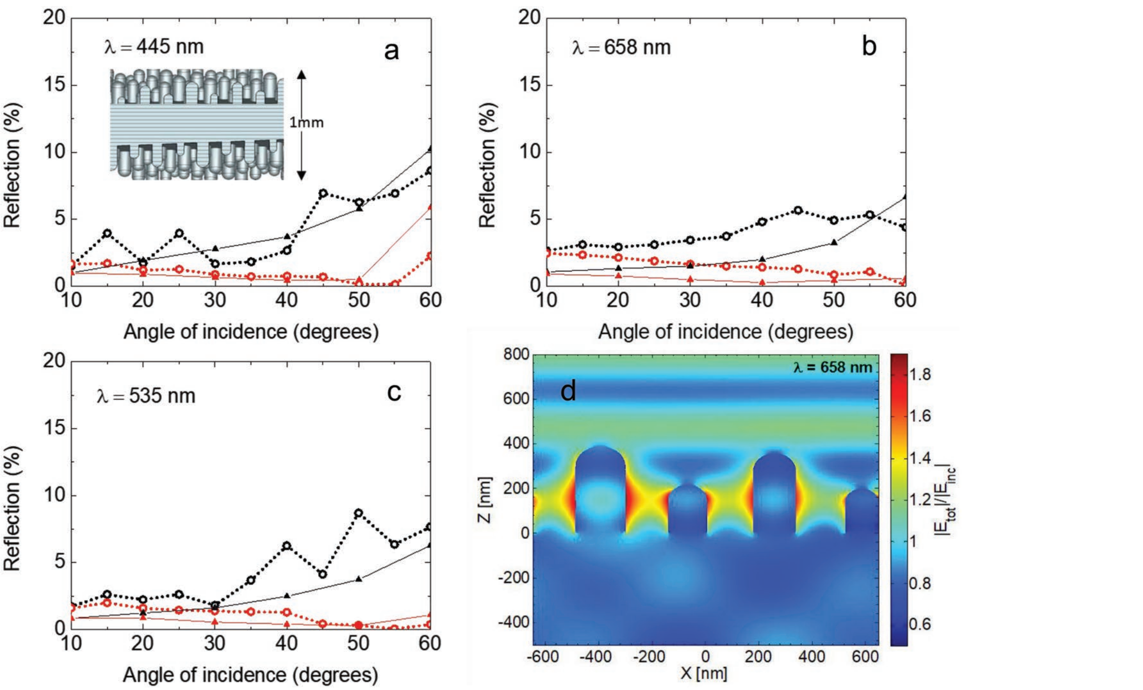

Figure 5. Theory (dashed line) versus experiment (continuous line). a–c) Reflectance measurements for various AOI at 445 nm (a), 658 nm (b), and 535 nm (c) wavelengths of single-side processed (black) and double-side processed (red) fused silica. d) Distribution of electric field $|\bar{E}|$ at a wavelength of 658 nm at normal incidence.

Our simulation analysis indicated that this random height distribution of nanospikes not only significantly reduces the surface reflectivity but also is the main reason for the observed broadband, omnidirectional antireflection property. Optical spectroscopy, indeed, confirmed that the reflectivity is suppressed by almost one order of magnitude over a large range of incident angles and wavelengths. More important, and contrary to the currently best antireflection technologies, the observed optical properties are found to be remarkably stable over time. Such a combination of efficient omnidirectional antireflective performance with high durability has not yet been achieved by any of the currently well-established AR technologies. Due to the nature of laser-processing technology, the antireflective surfaces can be easily scaled up to large areas that could be used to enhance the light harvesting in solar cells or for efficient light emission in light-emitting diodes, as well as improving the performance of optoelectronic and electro-optical components and devices, including mirrors, lenses, photodetectors, and displays.[31,33,48]

Experimental Section

Laser Processing: Commercially available, UV-grade polished samples of fused silica of 99.9% purity (purchased from GPO, Germany), with an average thickness of 1 mm, were used. For the fabrication procedure, a potassium gadolinium tungstate (Yb:KGW) laser source emitting linearly polarized pulses with a pulse duration of 170 fs, 1 kHz repetition rate, and 1026 nm central wavelength, was employed. To produce left-handed circularly (LC) polarized pulses, a quarter-waveplate (QW) plate was used, where the optical axis was set to 45° with respect to the original linear polarization. The experimental setup, shown in Figure S14 (Supporting Information), also included a system of a half-waveplate (HW) and a linear polarizer (LP), used to adjust the laser power, a dichroic mirror (DM) to guide the beam, a concave lens (CL) of focal length $f = 150$ mm to focus the beam onto the sample, and a complementary metal–oxide–semiconductor (CMOS) camera to observe the sample surface. The sample was placed on a computer controlled three-axis translational stage. The spot size was calculated to be 41 µm in diameter at $1/e^2$ using a CCD camera. All experiments were conducted in ambient air, at normal incidence, and tight focusing conditions.

Morphological and Optical Characterization: The morphology of the laser-fabricated structures was analyzed by a field-emission SEM (JEOL JSM-7000F). The periodicity of surface structures was determined by the 2D-FFT analysis of the corresponding SEM images using the Gwyddion software (Section SA, Supporting Information), while the radius and height of the structures were calculated from the SEM images via the ImageJ software. The reflectivity of the flat and the processed surface areas was measured via a Bruker Vertex 70v FT-IR vacuum spectrometer, using a PIKE specular reflectance sample holder with a fixed 30° angle of incidence. In order to cover a spectral range of 22 500–4000 cm^{-1} (444–2500 nm), two different sets of optics were used: a) for 22 500–8000 cm^{-1} (444–1250 nm), a quartz beamsplitter and a room-temperature silicon diode detector; while b) for 7500–4000 cm^{-1} (1333–2500 nm), a broadband KBr beamsplitter and a room-temperature broadband triglycine sulfate (DTGS) detector were used. In any case, interferograms were collected at 4 cm^{-1} resolution (8 scans), apodized with a Blackman–Harris function, and Fourier transformed with two levels of zero filling to yield spectra encoded at 2 cm^{-1} intervals. Before scanning the samples, an aluminum mirror (>90% average reflectivity) background measurement was recorded in vacuum. Finally, the transmittance and reflectance of the processed areas at various angles of incidence were measured at 445, 535, and 648 nm wavelengths, emitted by respective continuous wave (cw) laser sources.

Supporting Information

Supporting Information is available from the Wiley Online Library or from the author.

Acknowledgements

A.P. and E.Sk. have equal contribution in designing and performing the experiments and the characterization. A.M. performed experiments on other types of glasses. G.D.T., G.P. and G.K. have performed the theoretical modeling and simulations. E.St conceived the idea and was in charge of overall direction, planning and supervision. E.St also wrote the paper with input from all authors. This work was supported by the project LiNaBioFluid, funded by EU's H2020 framework program for Research and Innovation (Grant Agreement No. 665337) and from Nanoscience Foundries and Fine Analysis (NFFA)–Europe H2020-INFRAIA-2014-2015 (Grant agreement no. 654360). Funding was also acknowledged from the General Secretariat for Research and Technology (GSRT) and Hellenic Foundation for Research and Innovation (HFRI) (Grant No. 130229/I2). The authors acknowledge the technical support and software development by A. Lemonis (scilabs.gr), also G. Aerakis and Dr. A. Trichas, Arthropod Collections Curator, NHMC for their useful insight concerning the Cicada *Cretensis* species identification.

Conflict of Interest

Part of the findings of this study has been submitted as a patent with international application number PCT/GR2018/000010 and are planned to be exploited by a spin-off company of FORTH, called Biomimetic. The authors declare no conflict of interest.

Keywords

antireflection, biomimetic, glass, nanostructuring, ultrafast lasers

Received: February 18, 2019
Revised: April 29, 2019
Published online:

[1] C. Neinhuis, W. Barthlott, *Ann. Bot.* **1997**, *79*, 667.
[2] J. Morikawa, M. Ryu, G. Seniutinas, A. Balčytis, K. Maximova, X. Wang, M. Zamengo, E. P. Ivanova, S. Juodkazis, *Langmuir* **2016**, *32*, 4698.
[3] R. H. Siddique, G. Gomard, H. Hölscher, *Nat. Commun.* **2015**, *6*, 6909.
[4] P. Vukusic, J. R. Sambles, *Nature* **2003**, *424*, 852.
[5] P. Comanns, C. Effertz, F. Hischen, K. Staudt, W. Böhme, W. Baumgartner, *Beilstein J. Nanotechnol.* **2011**, *2*, 204.
[6] L. Wen, J. C. Weaver, G. V. Lauder, *J. Exp. Biol.* **2014**, *217*, 1656.
[7] E. I. Stratakis, V. Zorba, in *Nanotechnologies for the Life Science*, Vol. *7* (Ed: C. S. Kumar), Wiley-VCH, Weinheim, Germany **2012**, pp. 379–428.
[8] Y. F. Huang, S. Chattopadhyay, Y. J. Jen, C. Y. Peng, T. A. Liu, Y. K. Hsu, C. L. Pan, H. C. Lo, C. H. Hsu, Y. H. Chang, C. S. Lee, K. H. Chen, L. C. Chen, *Nat. Nanotechnol.* **2007**, *2*, 770.
[9] P. B. Clapham, M. C. Hutley, *Nature* **1973**, *244*, 281.
[10] A. Rahman, A. Ashraf, H. Xin, X. Tong, P. Sutter, M. D. Eisaman, C. T. Black, *Nat. Commun.* **2015**, *6*, 5963.
[11] H. Savin, P. Repo, G. von Gastrow, P. Ortega, E. Calle, M. Garín, R. Alcubilla, *Nat. Nanotechnol.* **2015**, *10*, 624.
[12] E. Stratakis, H. Jeon, S. Koo, *MRS Bull.* **2016**, *41*, 993.

[13] E. Skoulas, A. Manousaki, C. Fotakis, E. Stratakis, *Sci. Rep.* **2017**, *7*, 45114.

[14] U. Hermens, S. V. Kirner, C. Emonts, P. Comanns, E. Skoulas, A. Mimidis, H. Mescheder, K. Winands, J. Krüger, E. Stratakis, J. Bonse, *Appl. Surf. Sci.* **2017**, *418*, 499.

[15] F. Müller, C. Kunz, S. Gräf, *Materials* **2016**, *9*, 476.

[16] S. V. Kirner, U. Hermens, A. Mimidis, E. Skoulas, C. Florian, F. Hischen, C. Plamadeala, W. Baumgartner, K. Winands, H. Mescheder, J. Krüger, J. Solis, J. Siegel, E. Stratakis, J. Bonse, *Appl. Phys. A* **2017**, *123*, 754.

[17] V. Zorba, E. Stratakis, M. Barberoglou, E. Spanakis, P. Tzanetakis, S. H. Anastasiadis, C. Fotakis, *Adv. Mater.* **2008**, *20*, 4049.

[18] E. Stratakis, A. Ranella, C. Fotakis, *Biomicrofluidics* **2011**, *5*, 013411.

[19] E. Stratakis, *Sci. Adv. Mater.* **2012**, *4*, 407.

[20] A. Papadopoulos, E. Skoulas, G. D. Tsibidis, E. Stratakis, *Appl. Phys. A* **2018**, *124*, 146.

[21] G. D. Tsibidis, E. Skoulas, A. Papadopoulos, E. Stratakis, *Phys. Rev. B* **2016**, *94*, 81305.

[22] S. Höhm, A. Rosenfeld, J. Krüger, J. Bonse, *J. Appl. Phys.* **2012**, *112*, 014901.

[23] L. Jiang, X. Shi, X. Li, Y. Yuan, C. Wang, Y. Lu, *Opt. Express* **2012**, *20*, 21505.

[24] X. Shi, L. Jiang, X. Li, S. Wang, Y. Yuan, Y. Lu, *Opt. Lett.* **2013**, *38*, 3743.

[25] A. Borowiec, H. K. Haugen, *Appl. Phys. Lett.* **2003**, *82*, 4462.

[26] S. Chattopadhyay, Y. F. Huang, Y. J. Jen, A. Ganguly, K. H. Chen, L. C. Chen, *Mater. Sci. Eng., R* **2010**, *69*, 1.

[27] H. K. Raut, V. A. Ganesh, A. S. Nair, S. Ramakrishna, *Energy Environ. Sci.* **2011**, *4*, 3779.

[28] L. K. Verma, M. Sakhuja, J. Son, A. J. Danner, H. Yang, H. C. Zeng, C. S. Bhatia, *Renewable Energy* **2011**, *36*, 2489.

[29] Q. Yang, X. A. Zhang, A. Bagal, W. Guo, C.-H. Chang, *Nanotechnology* **2013**, *24*, 235202.

[30] J. Cai, L. Qi, *Mater. Horiz.* **2015**, *2*, 37.

[31] J. Sun, X. Wang, J. Wu, C. Jiang, J. Shen, M. A. Cooper, X. Zheng, Y. Liu, Z. Yang, D. Wu, *Sci. Rep.* **2018**, *8*, 5438.

[32] J.-Q. Xi, M. F. Schubert, J. K. Kim, E. F. Schubert, M. Chen, S.-Y. Lin, W. Liu, J. A. Smart, *Nat. Photonics* **2007**, *1*, 176.

[33] M. Cudzinovic, T. Pass, A. Terao, P. J. Verlinden, R. M. Swanson, in *Conf. Rec. Twenty-Eighth IEEE Photovolt. Spec. Conf. - 2000 (Cat. No.00CH37036)*, IEEE, Piscataway, NJ, USA **2000**, pp. 295–298.

[34] R. Prado, G. Beobide, A. Marcaide, J. Goikoetxea, A. Aranzabe, *Sol. Energy Mater. Sol. Cells* **2010**, *94*, 1081.

[35] F. Fraggelakis, G. Mincuzzi, J. Lopez, I. Manek-Hönninger, R. Kling, *Opt. Express* **2017**, *25*, 18131.

[36] F. Fraggelakis, G. Mincuzzi, I. Manek-Hönninger, J. Lopez, R. Kling, *RSC Adv.* **2018**, *8*, 16082.

[37] J. Choi, *J. Mech. Sci. Technol.* **2016**, *30*, 2707.

[38] A. Gombert, W. Glaubitt, K. Rose, J. Dreibholz, B. Bläsi, A. Heinzel, D. Sporn, W. Döll, V. Wittwer, *Sol. Energy* **2000**, *68*, 357.

[39] P. Yu, C.-H. Chang, C.-H. Chiu, C.-S. Yang, J.-C. Yu, H.-C. Kuo, S.-H. Hsu, Y.-C. Chang, *Adv. Mater.* **2009**, *21*, 1618.

[40] K. M. Rosfjord, J. K. W. Yang, E. A. Dauler, A. J. Kerman, V. Anant, B. M. Voronov, G. N. Gol'tsman, K. K. Berggren, *Opt. Express* **2006**, *14*, 527.

[41] A. Jannasch, A. F. Demirörs, P. D. J. van Oostrum, A. van Blaaderen, E. Schäffer, *Nat. Photonics* **2012**, *6*, 469.

[42] K. Pfeiffer, U. Schulz, A. Tünnermann, A. Szeghalmi, *Coatings* **2017**, *7*, 118.

[43] Z. Diao, M. Kraus, R. Brunner, J. H. Dirks, J. P. Spatz, *Nano Lett.* **2016**, *16*, 6610.

[44] A. Rudenko, J. P. Colombier, S. Höhm, A. Rosenfeld, J. Krüger, J. Bonse, T. E. Itina, *Sci. Rep.* **2017**, *7*, 12306.

[45] J. A. Quartau, P. C. Simões, *Biologia, Bratislava* **2005**, *60/5*, 489.

[46] A. Rudenko, J. P. Colombier, T. E. Itina, *J. Laser Micro/Nanoeng.* **2016**, *11*, 304.

[47] G. Marrocco, F. Capolino, in *Electromagnetics in a Complex World,* Vol. *96* (Eds: I. M. Pinto, V. Galdi, L. B. Felsen), Springer, Berlin, Germany **2004**, pp. 249–257.

[48] S. Ji, K. Song, T. B. Nguyen, N. Kim, H. Lim, *ACS Appl. Mater. Interfaces* **2013**, *5*, 10731.